MEASUREMENT OF LONGITUDINAL BUNCH PROFILE AND TWISS PARAMETERS IN SNS LINAC

A. Aleksandrov, C. Huang, Y. Liu, A. Shishlo, A. Zhukov,
Oak Ridge National Laboratory, Oak Ridge, TN 37830, USA

Abstract

We are reporting on the latest progress in the longitudinal beam profile and emittance diagnostics development at SNS. In order to characterize the longitudinal phase space of the beam in the SNS 1GeV proton linac the bunch profiles need to be measured with a few picoseconds accuracy. The original SNS set of diagnostics included only four interceptive Feschenko-style longitudinal profile monitors in the normal conducting part of the linac at 100MeV. Two recently added systems are: a non-interceptive laser scanner in the injector at 2.5MeV and a novel non-interceptive method for longitudinal Twiss parameters measurement using the beam position monitors in the Super Conducting Linac (SCL) at 300MeV. This paper presents details of these two diagnostics; discuss their performance, resolution limitations and future development plans.

INTRODUCTION

The SNS 340m long linac consists of a 2.5MeV RFQ, an 86 MeV Drift Tube Linac (DTL), a 185 MeV Coupled Cavity Linac (CCL), a 1GeV Super Conducting Linac (SCL) and associated transport lines. It accelerates H^- beam in one-ms-long pulses with 38 mA peak current, chopped with a 68% beam-on duty factor at a repetition rate of 60 Hz to produce 1.6 mA average current. The beam is bunched at 402.MHz frequency. Low loss operation with average beam power of 1MW and higher requires careful matching of RMS beam parameters in transverse and longitudinal planes. Longitudinal RMS bunch size shrinks in the process of acceleration from about 100ps at 2.5MeV to about 10ps at 1GeV. The baseline set of SNS linac beam diagnostics included three Bunch Shape Monitors (BSMs) [1] for measuring the longitudinal bunch profile in the beginning of the CCL. This location was selected to facilitate the optimal tuning of the transition between the 402.5MHz DTL and 805MHz CCL. These BSMs played an important role during the warm linac commissioning. It became clear during the commissioning that measuring the bunch profile at a single location is not sufficient for troubleshooting many potential problems. The longitudinal bunch parameters should be measured at every major transition in the linac: from injector to the DTL, at the frequency jump and at the transition from the warm linac to the superconducting linac. An ad hoc laser based longitudinal profile monitor [2] was built in the injector to verify the longitudinal emittance after the RFQ detuning event. Later, when unexpected beam losses in the SCL were discovered, one more BSM was added at the end of the CCL to measure longitudinal halo in attempt to explain the losses. Finally, the intra-beam stripping mechanism of the beam loss was discovered and confirmed [3], which suggests that the loss mitigation requires a careful matching of the bunch RMS Twiss parameters at the SCL entrance in all three dimensions. A single BSM at the CCL exit does not provide the required accuracy of Twiss parameters determination therefore we developed a novel method for measurement of longitudinal Twiss parameters using the SCL Beam Position Monitors (BPMs) [4]. As of today, the SNS linac has a comprehensive set of tools for measuring the longitudinal bunch parameters: a laser profile monitor in the injector, four BSMs in the warm linac and a BPM based technique in the SCL. We reported on the performance of the SNS BSM recently in [5]. In this paper we will describe operation of the two other systems.

LASER WIRE FOR LONGITUDINAL PROFILE MEASUREMENT

In the Laser Bunch Shape Monitor (LBSM) a train of short pulses of light from a mode-locked laser synchronized with the 5th sub-harmonic of 402.5MHz SNS beam frequency strip the electrons from the negative hydrogen ions. The number of the detached electrons is proportional to the ion density in the interaction region. The electrons are separated from the ions by the magnet and collected in the Faraday Cup as shown in Fig.1. By scanning the laser phase relative to the bunch phase the longitudinal bunch profile is measured.

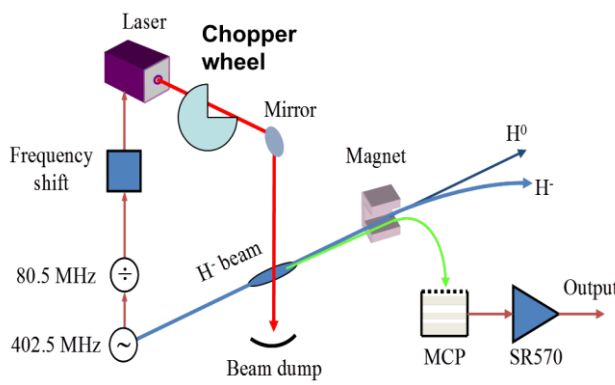

Figure 1: A layout of the Laser Bunch Shape Monitor.

The latest modifications of the LBSM system include replacement of a free propagation laser beam transport line with a 30m long fiber [6] and addition of a chopper wheel for an automated background subtraction. The

ISBN 978-3-95450-127-4

implementation of the fiber transmission line significantly improved the stability of the laser spot at the interaction point. As shown in Fig.2, the laser pulse width broadens after the propagation in the fiber but still remains within the acceptable range. In addition, the fiber output beam shows a well-defined Gaussian beam (Fig.3).

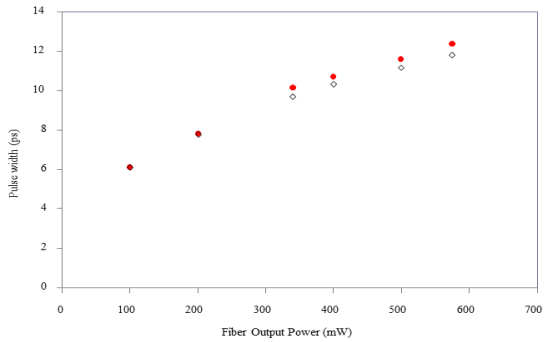

Figure 2: Laser pulse width after propagation through the 30-m long fiber vs. laser power.

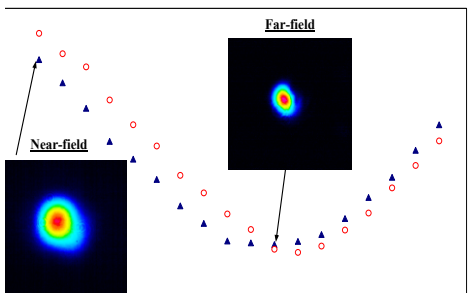

Figure 3: Laser spot size vs. distance from the collimation lens after the fiber propagation.

The electron detector consists of an in-vacuum dipole magnet mounted on a collection plate with an MCP amplifier. Parts of the detector are shown in Fig. 4.

A typical raw signal from the electron detector is shown in Fig. 5. It is dominated by X-Ray radiation from the nearbay RF cavity (the first step on the oscillogramm) and the electrons created by stripping on the residual gas (the second step). The two narrow peaks at the center of the trace correspond to the electrons ionized by the laser pulses. The level of the background signal is changing constantly with changing vacuum conditions therefore an automated background subtraction was implemented using a chopper wheel interrupting the laser beam for every other beam pulse. The performance of the background subtraction system is illustrated in Fig.6. Only the laser induced signal (magenta) remains after subtracting the background pulse (red) from the pulse with the laser open (blue).

Figure 4: The electron collector with an MCP amplifier (left) and the in-vacuum magnet (right).

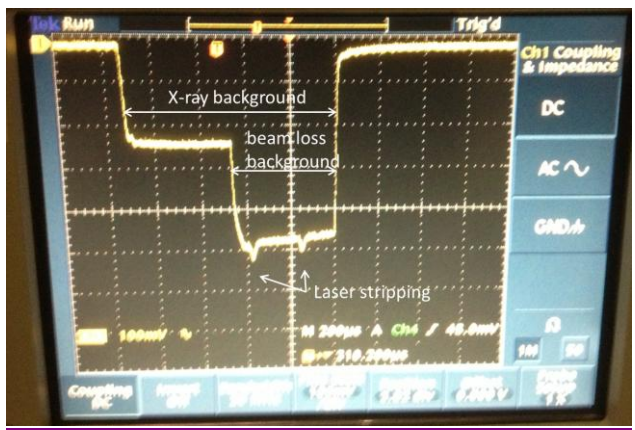

Figure 5: A typical raw signal from the electron detector.

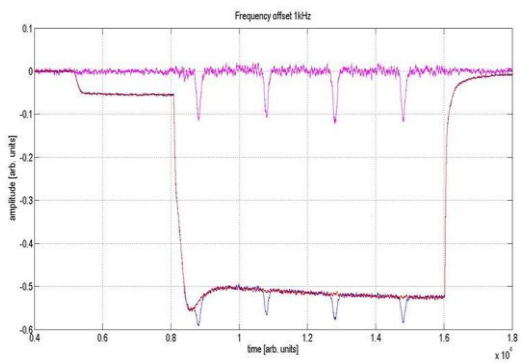

Figure 6: Illustration of the automated background subtraction using a chopper wheel (blue – laser is on; red – laser light is blocked by the chopper; magenta – laser induced signal without the background.

We use two methods of scanning the relative time between the laser pulses and the ion bunches: by changing the phase of the laser reference 80.5MHz signal with an electronic phase shifter (we call it the "phase scan_mode") or by introducing a small offset between the

ISBN 978-3-95450-127-4

laser reference frequency and the ion bunch train 5th sub-harmonic frequency. As a result, the laser pulse moves along the ion bunches train at a constant speed that is proportional to the frequency offset. We call it the "frequency shift mode". The frequency offset mode has several significant advantages: 1. The whole bunch profile is measured within a single beam pulse. 2. The absolute calibration is established by making the frequency offset large enough so that at least two profiles appear within the beam pulse. The distance between the two profiles is equal to the period of the ion bunches and sets the measurement scale. 3. The longitudinal profile at several locations along the beam pulse can be measured within one beam pulse as illustrated in Fig. 7.

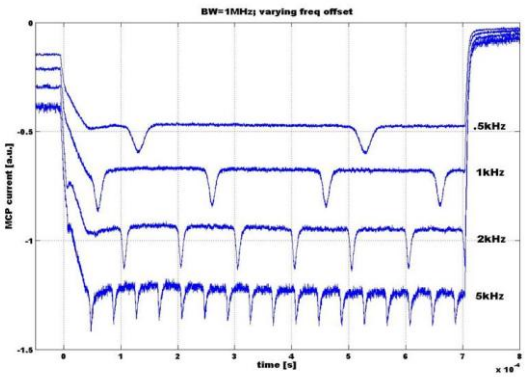

Figure 7: Bunch profile measurements with different frequency offsets in the frequency offset mode.

The maximum frequency offset is limited by the bandwidth of the laser synchronization circuit. For very short (<10-20μs) ion beam (macro-) pulses, the frequency offset mode will not work since the time interval is not sufficient for the laser pulse to scan over even a single ion bunch. In this case we use the phase scan mode, which requires multiple beam pulses to obtain a single bunch profile. The phase scan mode needs a careful calibration of the phase shifter to ensure high measurement accuracy. A typical phase scan measurement result is shown in Fig.8.

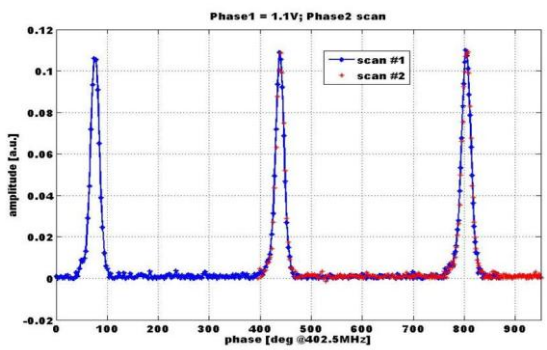

Figure 8: A typical bunch profile measurement in the phase scan mode.

DETERMINATION OF LONGITUDINAL TWISS PARAMETERS

The suggested new method for measuring the longitudinal Twiss parameters at the entrance of a superconducting linac is based on the analysis of the beam position monitor (BPM) sum signals [4]. These signals are proportional to the amplitude of the frequency spectrum of the longitudinal bunch distribution at the BPM's frequency. The unknown calibration constants can be measured directly during the nominal operation of the linac when bunch length is much shorter than the BPM operating frequency wavelength. Then the RF cavities are switched off and the bunch expands in free space. When its length becomes comparable with the BPM operating wavelength it can be easily calculated assuming the Gaussian longitudinal distribution. In the absence of space charge, the dependence of the rms bunch length upon the distance along the linac will be determined by the initial longitudinal Twiss parameters and the known transformation matrix of the drift. Therefore the Twiss parameters and their uncertainties can be found from the measured rms bunch lengths.

A typical result of the described above procedure is shown in Fig. 9. The model fits the experimental points well but, nonetheless, the errors on the found Twiss parameters are very large as shown in Table 1. These large uncertainties are caused by strong space charge repulsion in the bunch. In essence, the effect of the space charge on the bunch expansion is significantly larger than the influence of the initial Twiss parameters.

Table 1: Twiss Parameters at the SCL Entrance Calculated from Free Expanding Bunch Length

α	β [deg/MeV]	ε [MeV deg]
-.5±1.6	33±86	.7±4.2

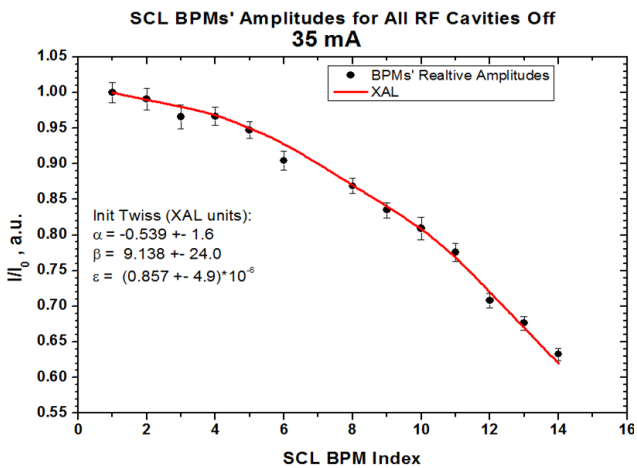

Figure 9: Attenuation of the 402.5MHz signal induced by the drifting bunch in the BPM vs. drift length (black – measurement; red –model).

ISBN 978-3-95450-127-4

In order to increase the effect of the initial Twiss parameters on the measured signals we can switch on the first accelerating cavity (SCL Cav01a in Fig.10) and perform a phase scan, while recording the BPM sum signal amplitude at each step. The layout of the measurement scheme is shown in Fig. 10. Then we fit the input Twiss parameters for the best agreement with the measured data.

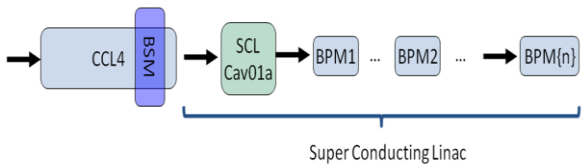

Figure 10: A layout of the longitudinal Twiss parameters measurement scheme.

A typical result of this procedure is shown in Fig. 11. The model fits the experimental points well and this time the errors on the found Twiss parameters are small as shown in Table 2.

Table 2: Twiss Parameters at the SCL Entrance Calculated from Free Expanding Bunch Length

α	β [deg/MeV]	ε [MeV deg]
-.56±.02	19.1±.5	.8±.01

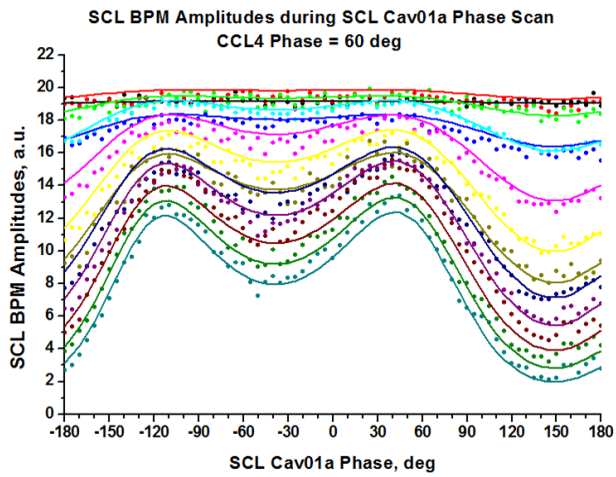

Figure 11: A typical result of the multiple BPMs response to the first cavity phase scan.

To verify the results of the Twiss parameters measurements we compared it with direct profile measurements in the nearby BSM. In order to provide comparison for a wide range of the Twiss parameters the phase of the CCL4 cavity was scanned. Each phase set point produced unique set parameters at the SCL entrance, which was measured using the above procedure. A model was used to propagate beam with the found Twiss parameters few meters upstream to the BSM location. Comparison of the RMS bunch lengths from the model with the BSM measurement is shown in Fig. 12. There is a good agreement in a wide range of CCL4 phases where the assumption of Gaussian bunch shape is justified.

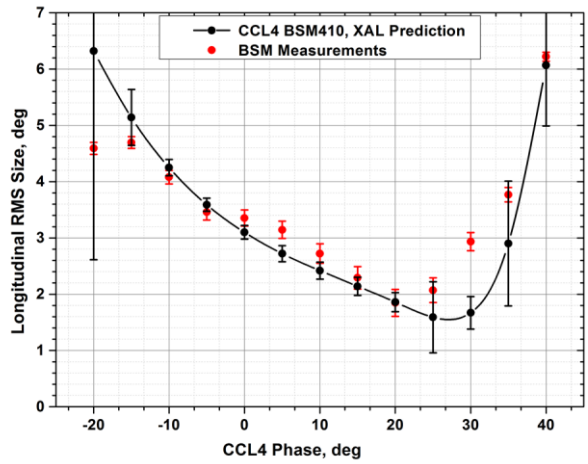

Figure 12: A comparison of bunch length obtained by two methods: direct measurement with BSM (red) and derived from the Twiss parameters measured in SCL (black).

ACKNOWLEDGEMENT

ORNL/SNS is managed by UT-Battelle, LLC, for the U.S. Department of Energy under contract DE-AC05-00OR22725.

REFERENCES

[1] A. Feschenko *et al.*, Proc. PAC2001, p. 517.
[2] S. Assadi *et al.*, Proc. EPAC 2006, p.3161.
[3] A. Shishlo *et al.*, Phys. Rev. ST Accel. Beams 16, 062801, (2013).
[4] A. Shishlo *et al.*, Phy. Rev. Lett. 108, 114801, (2012).
[5] A. Aleksandrov *et al.*, Proc. BIW2012, p.107.
[6] C. Huang *et al.*, APPLIED OPTICS / Vol. 52, No. 19, (2013), p.4462-4467.

ISBN 978-3-95450-127-4